Lignin-derived Lithiophilic Nitrogen-doped Three-dimensional Porous Carbon as Lithium Growth Guiding Layers for Lithium-metal Batteries

Nak Hyun Kim,[a,†] Merry Lee,[b,†] Hye Min Kwon,[a] Woo Hyeong Sim,[a] Donghyoung Kim,[a] Samick Son,[c] Ki Yoon Bae,[c] Ji Young Kim,[c] Duck Hyun Youn,[d] Yong Sik Kim,[e,*] and Hyung Mo Jeong [a,*]

**Corresponding authors: yongsikk@kangwon.ac.kr, hmjeong@skku.edu; † These authors contributed equally to this work.*

DOI: 10.15376/biores.19.1.1010-1029

GRAPHICAL ABSTRACT

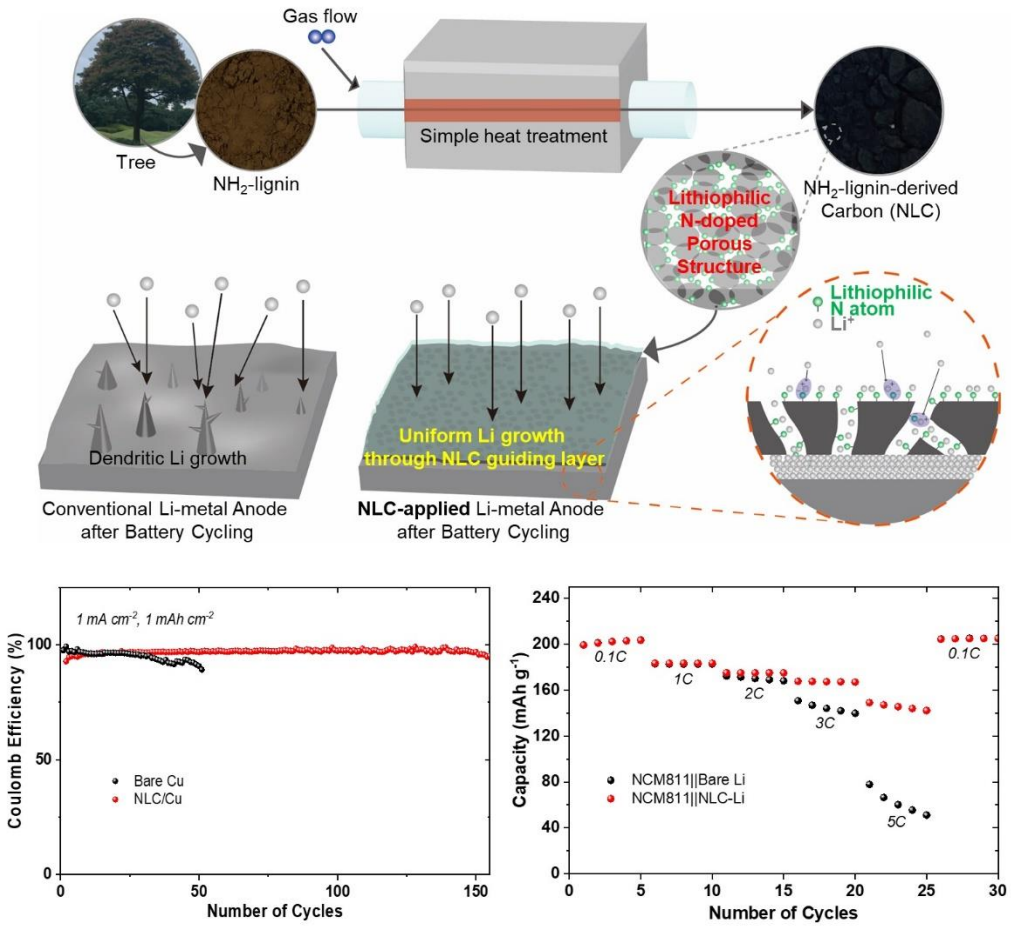

Lignin-derived Lithiophilic Nitrogen-doped Three-dimensional Porous Carbon as Lithium Growth Guiding Layers for Lithium-metal Batteries

Nak Hyun Kim,[a,†] Merry Lee,[b,†] Hye Min Kwon,[a] Woo Hyeong Sim,[a] Donghyoung Kim,[a] Samick Son,[c] Ki Yoon Bae,[c] Ji Young Kim,[c] Duck Hyun Youn,[d] Yong Sik Kim,[e,*] and Hyung Mo Jeong [a,*]

The growing demand for high-performance next-generation lithium (Li)-based batteries has brought Li-metal anodes into the spotlight, due to their high theoretical capacity (3,860 mAh g^{-1}) and low electrochemical potential (-3.04 V *vs.* SHE). However, the practical application of Li-metal anodes faces formidable challenges, primarily associated with dendritic Li growth resulting from non-uniform ion flux. Although previous studies utilizing carbonaceous materials having pores and lithiophilic atoms have demonstrated powerful performances, the complex process involving pore creation and doping with heteroatoms still has limitations in terms of cost-effectiveness. This study introduces a lithiophilic nitrogen (N)-doped three-dimensional (3D) porous carbon (NLC) by simply reusing and carbonizing NH_2-functionalized lignin (NL), an eco-friendly biopolymer derived from waste wood generated during the pulping process. The NLC offers macro-porous spaces with a rich array of N-doped sites, capable of accommodating and guiding Li deposition to facilitate uniform Li growth. The results demonstrate the effectiveness of the NLC as the Li growth guiding layer in Li-metal batteries. A full cell incorporating the NLC as a Li growth guiding layer, with NCM811 as cathodes, exhibits a remarkable capacity of 145. 57 mAh g^{-1} even at a high C-rate of 5C and capacity retention of 90.3% (167 mAh g^{-1}) after 150 cycles at 1C. These findings represent significant advancements compared to conventional Li-metal batteries.

DOI: 10.15376/biores.19.1.1010-1029

Keywords: Lithium-metal batteries; Lithium growth control; Lithiophilic sites; Lignin derived carbon; Functional layer

*Contact information: a: School of Mechanical Engineering and Department of Smart Fab. Technology, Sungkyunkwan University, 2066 Seobu-ro, Suwon-si, Gyeonggi-do, Republic of Korea; b: Department of Advanced Materials Science and Engineering, Sungkyunkwan University, 2066 Seobu-ro, Suwon-si, Gyeonggi-do, Republic of Korea; c: Advanced Battery Development Group, Hyundai Motor Company, 150, Hyundaiyeonguso-ro, Namyang-eup, Hwaseong-si, Gyeonggi-do, Republic of Korea; d: Department of Chemical Engineering, Kangwon National University, 1, kangwondaehak-gil, Chuncheon-si, Gangwon-do, Republic of Korea; e: Department of Paper Science and Engineering, Kangwon National University, 1, kangwondaehak-gil, Chuncheon-si, Gangwon-do, Republic of Korea; *Corresponding authors: yongsikk@kangwon.ac.kr, hmjeong@skku.edu; † These authors contributed equally to this work.*

INTRODUCTION

The increasing demand for high-performance batteries has accelerated the exploration of next-generation energy storage technologies beyond conventional lithium (Li)-ion batteries (Janek and Zeier 2016). The Li-metal anodes have emerged as pivotal

components in the development of next-generation Li-based batteries, due to their exceptional attributes, including a substantial theoretical capacity (3,860 mAh g^{-1}) and low electrochemical potential (-3.04 V *vs.* SHE) (Xu *et al*. 2014). These features lead to high capacity and high energy density in batteries, respectively. Nevertheless, the practical use of Li-metal anodes faces formidable challenges due to the formation of byproducts that impede reversible Li stripping/plating and the growth of dendritic Li induced by non-uniform ion flux during cycling. These challenges not only result in severe degradation in battery performance but also cause dendritic Li growth, leading to development of short-circuiting through a separator, accompanied by safety issues in the end.

Prior research has attempted to address these challenges by incorporating additives in electrolytes to establish a stable solid-electrolyte interphase (SEI) on Li-metal anodes (Togasaki *et al*. 2014; Li *et al*. 2016) or by inducing uniform Li deposition through modified separators (Huang *et al*. 2015; Tung *et al*. 2015). On the electrode side, the use of Li-hosting materials with three-dimensional (3D) porous structures has shown promise in enhancing the performance of Li-metal batteries (Lee *et al*. 2016; Yang *et al*. 2017), employing materials such as carbon (Zheng *et al*. 2014), copper (Yu *et al*. 2019), and nickel (Yue *et al*. 2018), among others. The increased surface area serves to reduce the partial current density at the electrode surface, further contributing to the uniformity of Li deposition (Chen *et al*. 2019). However, the use of transition metals can contribute to environmental pollution and incur high costs. Therefore, developing eco-friendly materials with cost-effective methods is crucial in the field of battery research.

Previous research into homogeneous Li-ion flux, utilizing environmentally friendly carbonaceous materials, has introduced a method involving the doping of heteroatoms (Wu *et al*. 2018), particularly those with lithiophilic properties, such as nitrogen (N) or oxygen (O) atoms (Sim and Jeong 2020). The incorporation of lithiophilic atoms is effective in guiding Li-ion flux at an atomic scale, resulting in uniform Li growth even under harsh conditions during battery operation. In this manner, porous structured carbonaceous materials with lithiophilic atoms not only can guide but also accommodate Li deposition, forming thoroughly uniform Li growth. Conventionally, pore creation and doping in carbonaceous materials are carried out separately, often involving complex processes or requiring the additional use of other materials, thereby raising costs (Inagaki *et al*. 2018; Wei *et al*. 2015; Sani *et al*. 2023).

Researchers have been passionate about reusing biomass generated in the environment in an eco-friendly way. Among them, lignin, a biopolymer extractable from waste wood during the recycled pulping process (Ponnusamy *et al*. 2019), has gained attention due to its relatively high carbon content and aromatic structure (Wang *et al*. 2019). Carbon materials derived from lignin, obtained through carbonization (Zhang *et al*. 2022), have been proposed for use as electrodes or coating layers in battery applications (Chen *et al*. 2022), thanks to their merits. However, the creation of a porous structure during carbonization necessitates the separate introduction of activation materials, which can be highly corrosive, such as potassium hydroxide (KOH), zinc chloride ($ZnCl_2$), or calcium carbonate ($CaCO_3$) (Wang *et al*. 2023). Additionally, the incorporation of N-doped carbon from lignin materials requires post-treatment involving several intricate stages following carbonization (Huang *et al*. 2021; Shi *et al*. 2022). Hence, the simplification of multiple steps, including carbonization, pore creation, and doping, is essential to enable the practical utilization of recycled biomaterials. Despite the numerous advantages of environmentally friendly biomass-derived carbons (Yan *et al*. 2023), there has been little research focused on their production through a cost-effective simple process, especially for

use in increasingly demanding Li-metal batteries.

Here, a straightforward approach is introduced involving a carbonization of a lignin with a NH_2-functional group (NH_2-lignin, NL) to produce lithiophilic N-doped 3D porous carbon (NLC). By applying the NLC as Li growth guiding layers to Li-metal batteries, the performance of the batteries is enhanced by effectively mitigating dendritic growth of Li. The inherent porous structure of the NLC offers a large surface area for transporting and accommodating Li-ions through its layer, while the diverse N atoms within its structure facilitate favorable interactions with Li-ions. This interaction aids in guiding Li-ions along with homogeneous Li-ion flux on an electrode surface (Sim and Jeong 2020; Won *et al*. 2023), thereby promoting uniform Li deposition. Consequently, in the result of a full cell test with NCM811 as cathodes, the NLC-applied Li-metal batteries show a notable capacity of 146 mAh g^{-1} even under a high C-rate of 5C and capacity retention of 90.3% (167 mAh g^{-1}) after 150 cycles at 1 C. In stark contrast, conventional Li-metal batteries exhibit a capacity of only 60 mAh g^{-1} at 5C and capacity retention of 84.6% (157 mAh g-1) after 150 cycles at 1C.

EXPERIMENTAL

Materials and Characterizations

Kraft lignin (KL, average M_w = 11,000 by GPC) was supplied by Moorim Pulp & Paper Co., Ltd., South Korea. To obtain NH_2-lignin, (3-aminopropyl)triethoxysilane (APTES, 99%) and anhydrous toluene (99.8%) were purchased from Sigma Aldrich. The NL was synthesized through a one-step reaction using APTES according to previous studies (An *et al*. 2020; Heo *et al*. 2022). Briefly, 1 g of KL was dispersed in 50 mL of anhydrous toluene. Subsequently, 9.0 mmol of APTES was added dropwise to the mixture under a nitrogen atmosphere and heated to 70 °C for 24 h. After the reaction, the mixture was filtered and washed several times with toluene to remove the unreacted APTES. Then, it was dried at 40 °C for 48 h to yield NH_2-lignin. (Note: see Supplementary Fig. 1 and Supplementary Table 1.) The carbonization process was conducted through heat treatment using a Chemical Vapor Deposition (CVD). The KL and NL were prepared in amounts of 400 mg each. Each sample was heated to 800 °C Celsius at a heating rate of 12 °C /min, held at 800 °C for 45 m, then further heated to 900 °C at a heating rate of 10 °C /min and maintained at 900 °C for 15 m. All heat treatments were carried out with a nitrogen flow of 20 standard cubic centimeter per minute (sccm).

The morphology of KL, NL, carbonized KL (KLC), and carbonized NL (NLC) particles and their surface of electrode were observed by scanning electron microscope (SEM, SUPRA55VP, Carl Zeiss) and transmission electron microscope (TEM, JEM-2100F, JEOL). The characteristics of pores were examined by Brunauer-Emmett-Teller (BET, Surface area analyzer, ASAP2420, Micromeritics). Other characteristics were investigated through X-ray diffractometer (XRD, SmartLab, Rigaku), Raman spectroscopy with 532 nm-laser (XperRAM-S567, Nanobase), Fourier transform infrared (FTIR, FT/IR4700, JASCO), and X-ray photoelectron spectroscopy (XPS, K Alpha+, Thermo Scientific). The XRD was conducted with a scan for 1 h for each sample. The Raman spectroscopy was performed after calibration using standard silicon material. The FTIR was conducted in the useful attenuated total reflection (ATR) mode. The XPS data were interpreted considering that all the peaks shift with the representative C-C bond peak position (284.6 eV).

The molecular weights were determined using gel permeation chromatography (GPC, Shimadzu-20A). The measurements were conducted with an eluent system consisting of DMF containing 0.1% LiBr. The elemental composition of the synthesized products was detected using an elemental analyzer (Flash EA 1112, Thermo Fisher Scientific) with a thermal conductivity detector, and 2,5-bis(5-tert-butyl-benzoxazol-2-yl)thiophene was used as the standard. After conducting the analysis using the GPC instrument, the obtained number average and weight average were calculated using the following formulas:

$$Mn = \frac{\sum N_i M_i}{\sum N_i}, Mw = \frac{\sum N_i {M_i}^2}{\sum N_i M_i} \quad (1)$$

Preparations of Li growth Guiding Layers for Li-metal Batteries

To make Li growth guiding layers of KLC and NLC, as-prepared KLC (or NLC) powder was dissolved in ethanol solvent, with Nafion D520 (5% w/w in water and 1-propanol, >1.00 meq g^{-1} exchange capacity, Alfa-Aesar Corp.), where a mass ratio of KLC (or NLC) and nafion was 80:20 (w/w). These slurries were casted on a Cu foil (UACJ Foil Corp.) and Celgard 2400 separator (monolayer polypropylene) using a doctor blade and dried in a vacuum oven at 60 ℃ overnight. After that, the KLC (or NLC)-coated Cu foil and separator were roll-pressed with a heat. The specifications for the guiding layer were produced according to the same standards used in previous research on additional layers for Li-metal batteries (Sim and Jeong 2021; Kwon *et al.* 2024).

Cell Fabrications and Electrochemical Measurements

CR2032 coin cell batteries were fabricated with 18 mm-diameter of Celgard2400 separator. In a half-cell, 14 mm-diameter of Cu foil and 12 mm-diameter of Li foil (Honjo Chemical Corp.) were used as the working and counter/reference electrode, respectively. In a symmetric cell, 12 mm-diameter of Li foil pieces were used as both working and counter/reference electrode. In a full cell, 10 mm-diameter of NCM811 (ROV Corp. and Posco Chem.) and 13 mm-diameter of Li foil were used as the working and counter/reference electrode, respectively.

NCM811 powder, graphite & carbon Super P® conductive carbon black (SUP-C65, Timcal), and poly(vinylidene fluoride binder) (Sigma-Aldrich®) with a ratio of 90:5:5 wt.% were mixed in N-methyl-2-pyrrolidone solvent and then casted on a Al foil (Welcos Corp.) using a doctor blade and dried in a vacuum oven at 60 ℃ overnight. After that, NCM811 cathodes were roll-pressed and punched, obtained with a mass loading of 5.85 to 8.01 mg cm^{-2}.

The standards for cell fabrication and electrochemical testing were conducted following the same procedures outlined in previous papers on additional layers for Li-metal batteries (Kwon *et al.* 2024; Sim and Jeong 2021). In the half-cell and symmetric cell, 120 uL of 1 M LiTFSI in 1:1 (by volume) DOL/DME (Enchem.) with 2 wt.% of $LiNO_3$ (ReagentPlus, Sigma-Aldrich®) was used as an electrolyte. In the full cell, 130 uL of 1.15 M $LiPF_6$ in 2:4:4 (by volume) EC/EMC/DMC + 1 wt.% VC + 1 wt.% $LiPO_2F_2$ was used (Welcos Corp.) as an electrolyte. All processes for fabricating cells were carried out in an argon (Ar)-filled glove box with oxygen (O_2) and water (H_2O) level <1 ppm.

WBCS3000 WonATech battery cyclers were used to perform electrochemical tests. The half-cells were tested at various current density and areal capacity with cutoff voltage up to 1.5 V, after 10 cycles at current density of 100 μA cm^{-2} from 0.02 to 1.0 V. The symmetric cells were tested at a current density 1.0 mA cm^{-2} and an areal capacity 1.0 mAh

cm^{-2}. The full cells for cyclability tests were firstly cycled at C/10 for 3 cycles and then cycled at 1C (1C is 200 mA g^{-1}) within a potential range of 2.7 to 4.3 V. All the cells were rested for 10 h before testing. The electrolyte for the cell was determined based on previous studies (Das *et al.* 2023).

RESULTS AND DISCUSSION

Nitrogen-doped Three-dimensional Porous Carbon Simply Derived from NH_2-lignin

Figure 1a depicts the carbonization process of NL, obtained from a tree. Through a simple carbonization process without additional dopant source and sacrificial template, necessary for doping and pore creation in carbon materials as reported in previous studies (Wei *et al*. 2015; Inagaki *et al*. 2018; Sani *et al*. 2023), the facile production of lithiophilic N-doping and a 3D porous structure is generated in NLC simultaneously, as illustrated in Fig. 1b. Figure 1c shows a conventional issue with Li-metal anodes in Li-metal batteries, characterized by dendritic Li growth due to the non-uniform Li-ion flux during Li deposition. When the NLC is introduced as a functional layer to guide uniform Li growth (Fig. 1d), a transformative effect is expected. Now, Li can be deposited onto an electrode in a stable and uniform manner, with the aids of not only favorable interactions inherent in lithiophilic N atoms but also the large surface area inherent in the 3D porous structure, guiding and accommodating Li-ions, as illustrated in Fig. 1e.

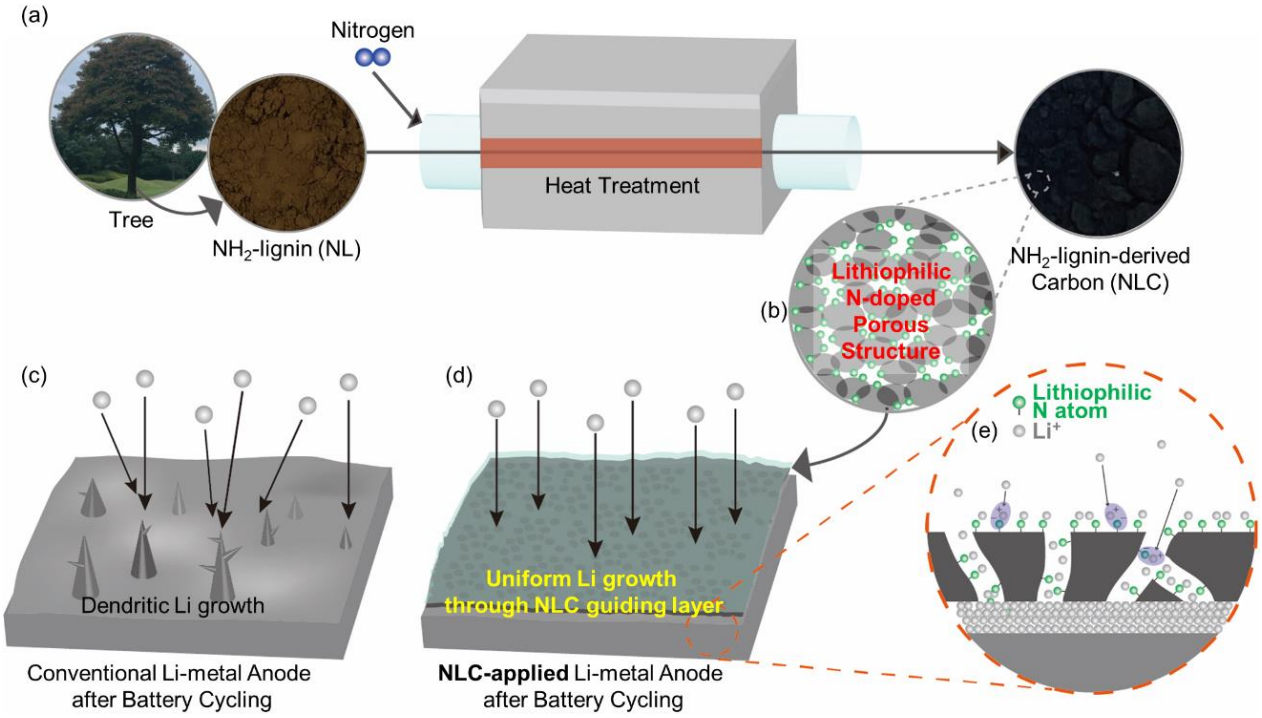

Fig. 1. Schematic illustrations of N-doped 3D porous carbon as Li growth guiding layer for Li-metal batteries. (a) Carbonization of NH_2-lignin, (b) N-doped porous structure of NH_2-lignin carbon, (c) Dendritic Li-growth in conventional Li-metal batteries, (d) Uniform Li-growth through functional layer of NH_2-lignin carbon, and (e) its Li deposition process

To comprehensively understand this study and the material characteristics, two distinct lignins were prepared: NL, enriched with NH_2-funcional groups, and KL, devoid of any added functional groups (Note: the molecular structures of these materials are provided in Supplementary Fig. 2.). An examination of their morphologies following carbonization, conducted using SEM, revealed notable distinctions between the two (Fig. 2a,b). Although both KL and NL underwent the same carbonization process, the morphological features of carbonized NL (NLC) clearly illustrated a fragmentation of particles into smaller entities, resulting in the formation of a porous structure (Fig. 2a-ii, b-ii). In contrast, the morphology of carbonized KL (KLC) closely resembled that of original KL (Fig. 2a-i, b-i). Further insight into the structural differences is provided by TEM images, as shown in Fig. 2c. The NLC exhibited the presence of small particles, approximately 100 nm in size, interconnected with one another, forming porous spaces (Fig. 2c-ii). In contrast, KLC displayed a lump of several micrometer-sized particles (Fig. 2c-i).

To analyze the pore structure, BET analysis was conducted, as shown in Fig. 2d. The BET isotherm (Fig. 2d-i) typically delineates three main regions, comprising micro-porous (<2 nm), meso-porous (2 to 20 nm), and macro-porous spaces (>20 nm) (Soboleva *et al*. 2010). Both KLC and NLC exhibited increased pore volume in micropores (initial increase in lower relative pressure (P/P_0)) and mesopores (slight increase in the middle P/P_0 region). Notably, when P/P_0 exceeded 0.95, only NLC exhibited a more pronounced increase in pore volume (Note: see the red circle marked in Fig. 2d-i), indicating the presence of numerous macropores within NLC, a direct outcome of its 3D porous structure. Consequently, the calculated BET surface area for NLC was 536 $m^2 g^{-1}$, surpassing that of KLC, which stands at 227 $m^2 g^{-1}$. Additionally, specific pore size distributions are shown in Fig. 2d-ii. Both KLC and NLC exhibited similar pore size distributions in microporous and mesoporous features within their structures, highlighting the main difference of the 3D porous structure in NLC resulting from macropore creation. The micropores and mesopores present in both KLC and NLC are attributed to some defect generation along with heat treatment during carbonization (Inagaki *et al*. 2018). However, the observed macroporous characteristics in NLC are primarily attributed to the presence of NH_2-functional groups in NL. These functional groups are thought to initiate further gas evolution without the need for any activating reagents, thereby contributing to the formation of a macroporous structure (Phothong *et al*. 2021), as evidenced by the interconnected 3D porous structure depicted in the morphological studies above. This interconnected 3D porous structure, consisting of multiple-scale pores in NLC, can play a significant role in facilitating the mass transport and diffusion of Li-ions through the NLC as additional functional layers for Li-metal batteries (Liu *et al*. 2023).

In the characterizations of other features on lignin-derived carbons, Fig. 2e presents the results of XRD for KL, KLC, NL, and NLC. Both KL and NL exhibited the (002) peak characteristic of randomly oriented layered graphitic carbon structures (Zou *et al*. 2006). Following the carbonization process, both KLC and NLC displayed a newly emerged (100) peak associated with carbon atoms residing on the same plane level (Zheng *et al*. 2022). This illustrates the typical characteristic of the carbon materials. Concurrently, the extent of defects in the carbon materials can be assessed by evaluating the ratio of the intensity of the D band to the G band (I_D/I_G) in Raman spectroscopy (Zheng *et al*. 2022). As depicted in Fig. 2f, the I_D/I_G value for NL was 0.961, slightly higher than that of KL (0.833), owing to the presence of N and silicon (Si) atoms in NL (Supplementary Fig. 2b).

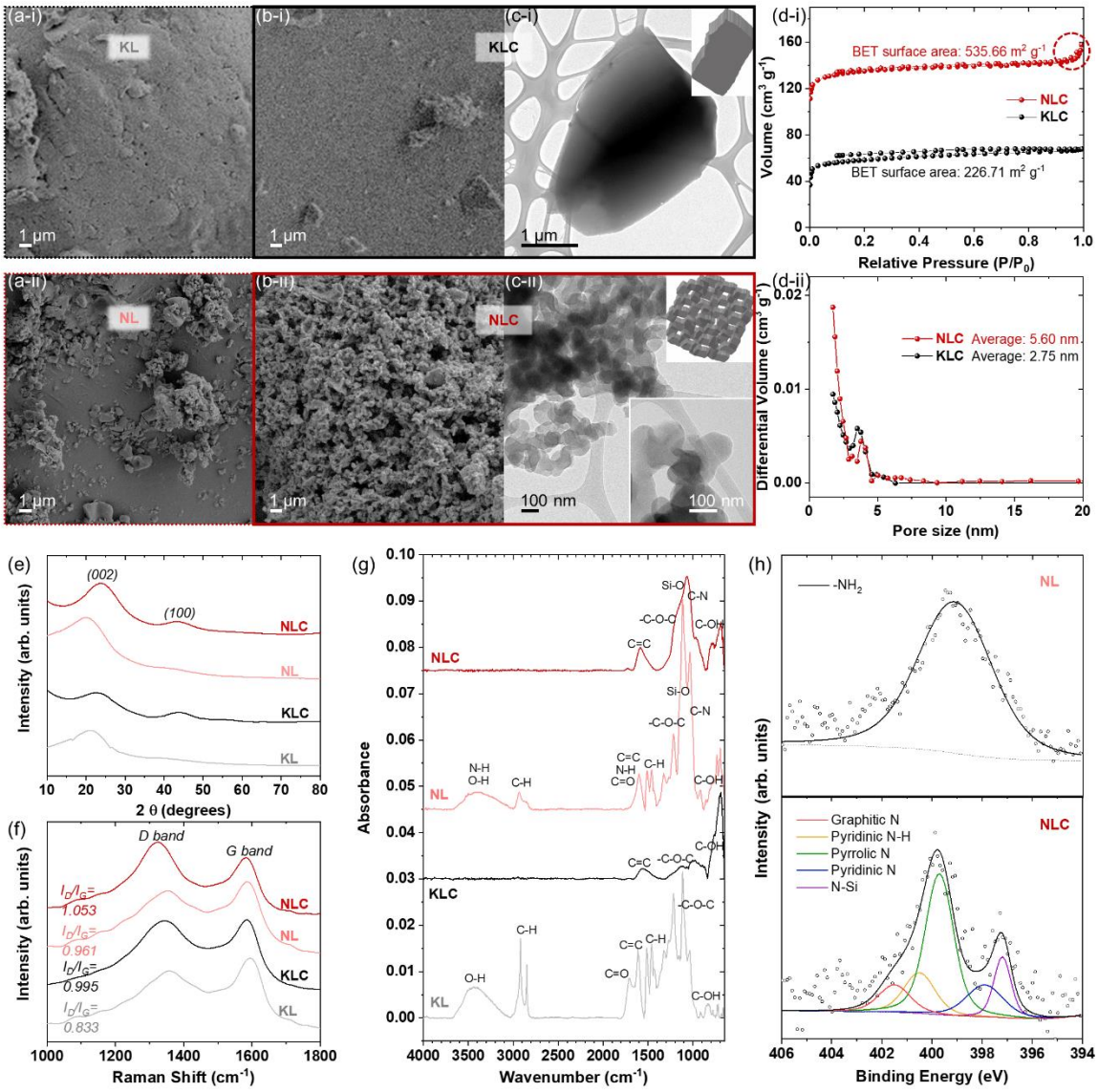

Fig. 2. Characterizations of kraft lignin (KL), NH_2-lignin (NL), and their carbons (KLC and NLC): (a) SEM images of (i) KL and (ii) NL. (b) SEM images of (i) carbonized KL (KLC) and (ii) carbonized NL (NLC). (c) TEM images of (i) KLC and (ii) NLC with schematic illustrations of each particle (inset). Results of (d) BET, (e) XRD, (f) Raman, (g) FTIR, and (h) XPS

After carbonization, the I_D/I_G values for both KL and NL increased up to 0.961 for KLC and 1.053 for NLC, indicating defect generation including the pore creation during the carbonization process.

Figure 2g shows the results of FTIR spectroscopy for KL, KLC, NL, and NLC. In the high wavenumber range (3670 to 2750 cm^{-1}), the absorbance peak corresponds to the vibration of O-H, N-H, and C-H bonds, while in the low wavenumber range (1840 to 650 cm^{-1}), the peak is associated with the vibration of C=O, N-H, C=C, C-N, C-O-C, Si-O, C-N, and C-OH bonds (Fan *et al*. 2021; Shokrani Havigh and Mahmoudi Chenari 2022; Zheng *et al*. 2022). Although NL contains N-H and C-N functionalities (Supplementary Fig. 2b), their peaks cannot be distinctly differentiated due to the predominance of O-H, C-H, C=O, C=C, and C-O-C peaks. After carbonization, both KLC and NLC exhibited the disappearance of peaks related to C-H, O-H, and N-H in the high wavenumber range (3670

to 2750 cm^{-1}). Simultaneously, peaks remained at 700 cm^{-1} (for both NLC and KLC), 1580 cm^{-1} (for NLC), and 1560 cm^{-1} (for KLC), indicating the persistence of C-OH and C=C. Notably, NLC exhibited a pronounced intensity in the 1250 to 880 cm^{-1} range even after carbonization, suggesting the presence of bonds involving N atoms in its structure.

To investigate the nature of the N chemical bons in NL and NLC further, XPS analysis was conducted, as shown in Fig. 2h. The NL exhibited an obvious peak at 399.2 eV, corresponding to its NH_2-functional groups (Supplementary Fig. 2b). After carbonization, the analysis unveiled a diverse array of lithiophilic N atoms within NLC. The N atoms within NLC include graphitic N (401.5 eV), pyridinic N-H (400.5 eV), pyrrolic N (399.7 eV), pyridine N (397.9 eV), and N-Si (397.2 eV) (Lazar *et al*. 2019; Ma *et al*. 2007). These diverse lithiophilic N atoms capable of interacting with Li-ions can be expected to play a crucial role in ensuring uniform Li growth by guiding Li-ions with a homogeneous Li-ion flux (Sim and Jeong 2020). Among the N atoms, pyrrolic and pyridinic N atoms have an unshared electron pair, and graphitic N atom and N atom in pyridinic N-H have a non-covalent electron (Supplementary Fig. 3). These electrons can strongly attract Li cations during Li deposition, which is called lithiophilic property. Therefore, these can play a crucial role in ensuring uniform Li growth by guiding Li-ions on an atomic scale with a homogeneous Li-ion flux (Sim and Jeong 2020). In stark contrast, examination of KLC *via* XPS revealed no bonds involving N atoms (Supplementary Fig. 4b). Considering NLC, characterized by lithiophilic N-doped 3D macroporous structure, it can function as an effective additional layer in facilitating Li deposition through the layer, leading to mitigating dendritic Li growth. This, in turn, contributes to the enhanced performance of Li-metal batteries.

Mitigating Dendritic Li Growth Through Li Growth Guiding Layers of Nitrogen-doped Three-dimensional Porous Carbon

In a battery test, the effects of additional layers for metal anodes were investigated through a half-cell configuration with a Cu foil as working electrodes and Li metal as counter/reference electrodes (Supplementary Fig. 5a). To verify the effectiveness of N-doped 3D porous carbon of NLC as an additional layer for guiding Li growth on electrode surfaces, NLC was introduced onto Cu foil (NLC-coated Cu foil, NLC/Cu) and half-cells using NLC/Cu were fabricated. The half-cells using bare Cu foil and KLC-coated Cu foil (KLC/Cu) were also fabricated for comparative purposes. Figures 3a–c show the results of electrochemical half-cell testing under different conditions, specifically varying current densities and areal capacities: (i) 1 mA cm^{-2} and 1 mAh cm^{-2}, (ii) 2 mA cm^{-2} and 1 mAh cm^{-2}, and (iii) 1 mA cm^{-2} and 2 mAh cm^{-2}.

Conventionally, a half-cell is initially tested under a current density of 1 mA cm^{-2} and an areal density of 1 mAh cm^{-2}, with subsequent variations for further examinations. Under these conditions, the amount of Li deposition on a working electrode corresponds to the Li deposition for 1 h under a speed of 1 mA cm^{-2}. (Note: under a current density of 2 mA cm^{-2} and an areal capacity of 1 mAh cm^{-2}, the amount of Li deposition on a working electrode corresponds to the Li deposition for 0.5 hours under a speed of 2 mA cm^{-2}. Additionally, under a current density of 1 mA cm^{-2} and an areal capacity of 2 mAh cm^{-2}, the amount of Li deposition on a working electrode corresponds to the Li deposition for 2 hours under a speed of 1 mA cm^{-2}.) Generally, when using half-cells under high current density (Li deposition rate) or high areal capacity (Li deposition amount), it is challenging to maintain high Coulomb efficiency over long cycles, which is an indicator of reversibility between Li deposition and removal on a Cu foil during discharge and charge, respectively.

Moreover, dendritic Li growth on a Cu foil can lead to short-circuiting, resulting in battery failure.

Remarkably, only NLC/Cu exhibited stable operation by consistently maintaining a high Coulomb efficiency of nearly 100% for 150 cycles under all conditions (Fig. 3a–c): a current density of 1 mA cm^{-2} and a further 2 mA cm^{-2} at the same areal capacity of 1 mAh cm^{-2} (Fig. 3a, b), and an areal capacity of 1 mAh cm^{-2} and a further 2 mAh cm^{-2} at the same current density (Fig. 3a, c). In contrast, bare Cu showed a short-circuit after about 110 cycles under the moderate Li deposition rate and amount (Fig. 3a), and a much shorter operation along with decreased Coulomb efficiency after about 30 cycles and 70 cycles under the high Li deposition rate and amount (Fig. 3b, c), respectively.

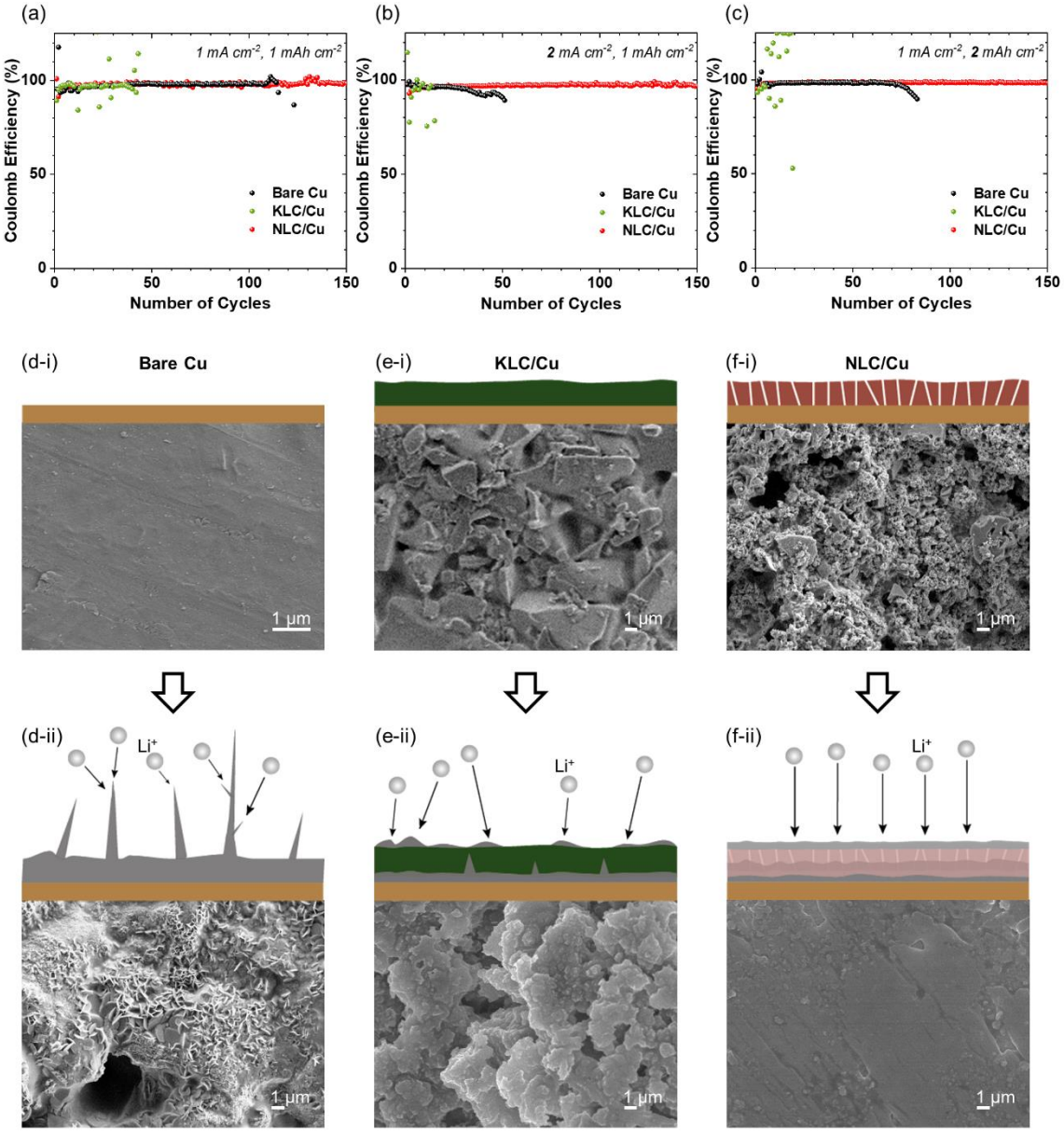

Fig. 3. Electrochemical characteristics on bare Cu, KLC on Cu (KLC/Cu), and NLC on Cu (NLC/Cu). (a–c) Results of an electrochemical half-cell testing. SEM images of (d) bare Cu, (e) KLC/Cu, and (f) NLC/Cu: (i) as prepared and (ii) after 50 cycles at 1 mA cm^{-2} and 1 mAh cm^{-2} (Li-plating state)

Meanwhile, KLC/Cu showed a very short operation for about 40 cycles along with unstable Coulomb efficiency under the moderate Li deposition rate and amount (Fig. 3a), and a short-circuit at the very first cycle under the high Li deposition rate (Fig. 3b) and a short-circuit even within 5 cycles under the high Li deposition amount (Fig. 3c). This outcome underscores the feasibility of achieving uniform Li growth and reversible Li deposition (plating) and removal (stripping) on the working electrode following battery discharge and charge, facilitated through the Li growth guiding NLC layer.

To gain insight into these observations, SEM investigations of the surfaces of bare Cu (Fig. 3d), KLC/Cu (Fig. 3e), and NLC/Cu (Fig. 3f) were conducted in two states: (i) as prepared and (ii) after Li deposition (after 50 cycles). In the case of bare Cu, a smooth surface was evident in the as-prepared state (Fig. 3d-i). However, after cycling, Li deposition with dendritic growth was observed (Fig. 3d-ii), a phenomenon that ultimately leads to cell short-circuiting. This result aligns with conventional Li-metal plating as reported in previous studies on Li-metal batteries (Sim and Jeong 2020; Won *et al*. 2023). On the other hand, the as-prepared KLC/Cu surface showed a rough texture with KLC particles (Fig. 3c-i). After cycling, Li was deposited non-uniformly on the surface of KLC particles without evident infiltration of Li from the KLC layer to the Cu foil (Fig. 3e-ii), resulting in unstable Coulomb efficiency at the very first cycle. Since the KLC layer lacks the ability to guide and transport Li-ions through its layer and allows limited Li-ion penetration due to the absence of the lithiophilic atoms and an interconnected pore structure (Liu *et al*. 2023) as discussed in the previous section, it acts like an ionic resistor for Li-ion transport.

Significantly, the as-prepared NLC/Cu surface displayed a porous structure (Fig. 3f-i) capable of guiding and transporting Li-ions through its rich array of lithiophilic N-doped 3D porous structure, as studied in the previous section. Consequently, it maintained a smooth surface with uniform Li deposition filled in the lithiophilic N-doped 3D porous structured NLC layer, even after repeated Li plating/stripping (Fig. 3d-ii). Notably, the interconnected pore structure consisting of multiple-scale pores facilitates Li-ion mass transport and shortens the Li-ion diffusion distance for Li plating (Liu *et al*. 2023), leading to powerful performance under the high Li deposition rate. Accordingly, the result in the high current density of 2 mA cm^{-2} (Fig. 3a-ii) revealed the most distinct differences among the three different Cu foils, with the NLC/Cu demonstrating the best performance. Furthermore, the lithiophilic N atoms interacted with Li-ions, facilitating their guidance within the porous structure, resulting in even and uniform Li deposition (Fig. 3d-ii). These findings spotlight the potential of NLC, obtained through a simple one-step process for recycling biomass, to significantly enhance the performance of Li-metal batteries by serving as an effective Li growth guiding layer.

Electrochemical Performance of Li-metal Batteries Using Nitrogen-doped Three-dimensional Porous Carbon as Li Growth Guiding Layers

To assess the practical applicability of the NLC effects in Li-metal batteries, symmetric cells using two identical Li-metal electrodes as working electrodes were fabricated as depicted in Supplementary Fig. 5b, and then electrochemical tests were conducted (Fig. 4a). In contrast to the previous half-cells used for electrochemically characterizing the NLC as Li growth guiding layers, symmetric cells with two identical working electrodes were employed to investigate electrode kinetics. This is a crucial aspect of practical battery performance that can help predict use of the NLC before testing practical full cell-configured Li-metal batteries (Yan 2023).

In the results (Fig. 4a), the bare Li exhibited a short-circuit only after 1000 h, accompanied by increasing overpotentials of 38.2, 78.6, 131.5 mV at 100, 500, 1000 h, respectively. This outcome is attiributed to dendritic Li growth during repeated Li stripping/plating, as observed in the SEM result in the previous section. One the other hand, the KLC-Li experienced a short-circuit shortly after 500 h, accompaynied by unstable overpotentials with 31.8 and 40.7 mV at 100 and 500 h, respectively.

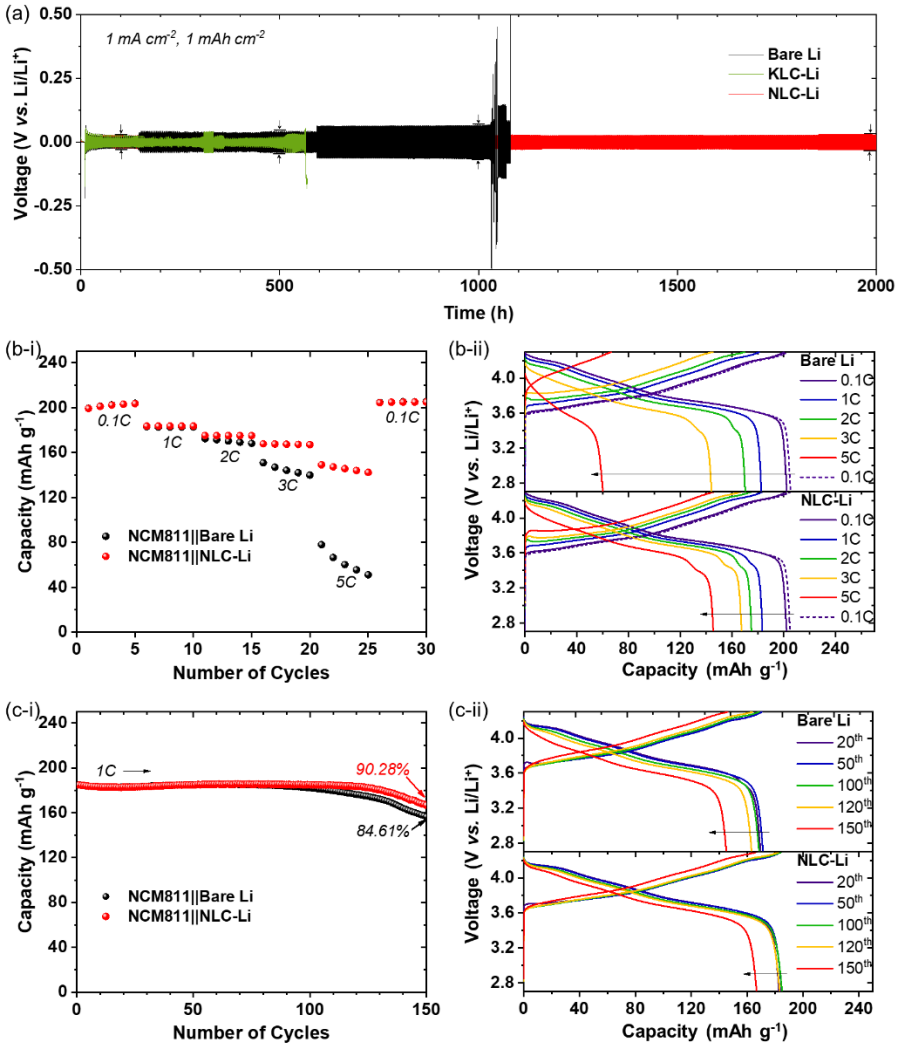

Fig. 4. Electrochemical performances of the NLC-applied Li-metal batteries. (a) Results of a symmetric cell testing for bare Li, KLC-Li, and NLC-Li, (b) Rate capabilities, and (c) cyclabilities of bare Li and NLC-Li in fabricating a full cell with NCM811 as cathodes: (i) Capacity-number of cycles and (ii) voltage profiles, respectively

The KLC-Li exhibited even greater instability compared to bare Li, which was the one without any additional layers for guiding Li growth. In contrast, the NLC-Li demonstrated remarkably stable cycling even up to 2000 h, maintaining consistently low overpotentials of 52.3, 67.6, 56.0, and 58.7 mV at 100, 500, 1000, 2000 h, respectively. This stability resulted from uniform Li deposition, mitigating dendritic Li growth. Moreover, the Li dendrite is often accompanied by the generation of dead Li which leads to battery degradation, including a safety issue during repeated cycling. Therefore, stable and uniform Li growth through additional Li growth guiding layers is much more important

for the practical use of Li-metal batteries (Xu *et al*. 2019). As confirmed by the half-cell results, the symmetric cell results spotlight the potential of NLC as Li growth guiding layers in practical Li-metal batteries.

Building upon the convincing findings described above, the next step was to fabricate full cells comprising bare Li and NLC-Li, coupled with NCM811 as the representative cathode, as illustrated in Supplementary Fig. 5c. (Note: the Li-metal as anodes and the NLC additional layer for guiding Li growth were introduced by coating on a commercial separator to physically adhere to the surface of Li-metal upon fabricating the full cell.) These cells were tested for checking rate capability (Fig. 4b) and cyclability (Fig. 4c) performances, which are indicators of representative battery performances regarding maintaining capacity retention under fast Li-ion moving rates between cathodes and anodes and over long cycles, respectively. Theoretically, 1C-rate (1C) means Li-ions move for 1 hour at a current density of 200 mA g^{-1}, based on the theoretical capacity of the used cathode (200 mAh g^{-1} for NCM811). Likewise, 2C means Li-ions move for 0.5 hours at 400 mA g^{-1}, and 0.5C means Li-ions move for 2 hours at 100 mA g^{-1}. Generally, under high C-rate or after long cycles, the battery underwent accelerated capacity fade accompanied by a degradation of electrodes.

In the rate capability results (Fig. 4b), the NLC-Li reveals the superior performance, along with a discharge capacity of 202, 184, 170, 167, and 146 mAh g^{-1} at the 3rd cycle of each of the respective C-rates: 0.1C, 1C, 2C, 3C, and 5C. In contrast, the bare Li showed discharge capacities of 202, 183, 170, 144, 60 mAh g^{-1} at the 3rd cycle for the corresponding C-rates. Particularly, a widening disparity was shown in discharge capacity at high C-rates (3C and 5C) between the NLC-Li and bare Li. Remarkably, the NLC-Li maintained a high capacity of 146 mAh g^{-1} even at 5C. This outstanding rate capability of the NLC-Li is attributed to facilitated Li-ion guidance and transportation through the NLC, within not only the larger surface area of the NLC layer, which reduces the partial current density experienced by Li-ions (Chen *et al*. 2019), but also promotes lithiophilic interactions, forming a homogeneous Li-ion flux (Sim and Jeong 2020), between Li-ions and diverse N atoms having unshared electrons in the NLC structure, as demonstrated in the previous XPS results.

Now, the cyclability test was conducted under a moderate C-rate of 1C (Fig. 4c). Although both the bare Li and NLC-Li showed similar discharge capacities at 1C in the rate capability results (Fig. 4b), these can widen the disparity after long cycles. In the cyclability results (Fig. 4c), both the bare Li and NLC-Li exhibited similar initial discharge capacities of 181 and 182 mAh g^{-1}, respectively. As the capacity fade proceeded during repeated cycling, bare Li showed a discharge capacity retention of 84.6% (157 mAh g^{-1}) after 150 cycles. In contrast, the NLC-Li demonstrated a higher discharge capacity retention of 90.3% (167 mAh g^{-1}) after 150 cycles compared to the bare Li despite being coupled with the naturally fast capacity-fading cathode of NCM811 usually after 50 cycles (Li *et al*. 2020). This improvement can be attributed to not only more uniform Li deposition facilitated by the additional NLC layer but also to the promotion of homogeneous Li-ion flux between cathodes and anodes. These results unequivocally confirm that lithiophilic N-doped 3D porous carbon derived simply from NH_2-lignin of the recycled biomass through the one-step process significantly enhanced the performances of both rate capability and cyclability in practical Li-metal batteries.

CONCLUSIONS

1. This study introduced N-doped 3D porous carbon (NLC), an eco-friendly carbonaceous material facilely derived from NH_2-lignin of recycled biomass through a simple, cost-effective carbonization process with heat treatment, as a highly effective Li growth guiding layer for Li-metal anodes in Li-metal batteries. The NLC exhibited an interconnected 3D macro-porous structure consisting of multiple-scale pores enriched with diverse lithiophilic N atoms having unshared electrons within its structure.
2. In electrochemical half-cell testing, the NLC significantly enhanced the uniform growth of Li, in stark contrast to conventional cells that suffered from short-circuits due to dendritic Li growth on the electrode surface. Symmetric cell testing further highlighted the advantages of NLC, as the Li-metal electrode with the assistance of NLC maintained consistently low overpotentials over 2000 h, while the conventional Li-metal electrode exhibited increasing overpotentials leading to short-circuits after 1000 h. Crucially, in full-cell testing, where NCM811 cathodes were employed, the cell incorporating the NLC-utilized Li-metal anode showed superior rate capability, delivering an impressive capacity of 146 mAh g^{-1} even under the high C-rate of 5C, in sharp contrast to the meager 60 mAh g^{-1} achieved by the conventional Li-metal anode. Furthermore, the NLC-Li demonstrated enhanced cyclability, retaining 90.3% (167 mAh g^{-1}) of its initial capacity after 150 cycles at 1C, surpassing the 84.6% capacity retention (157 mAh g^{-1}) observed for the conventional Li-metal anode after the same cycle counts.
3. The findings illuminate substantial advancements in practical Li-metal batteries through the incorporation of NLC as a Li growth guiding layer. This results from utilizing renewable materials of lignin from waste wood with a simple heat treatment after functionalization to have NH_2 groups. It is differentiated from previous studies that use complex processes for introducing pores and doped atom into carbonaceous materials. The incorporation of simultaneously produced lithiophilic atoms within a 3D porous structure contributed to enhanced battery performance based on eco-friendlier recycled carbons through a cost-effective approach. This opens a new avenue for the development of high-performance batteries utilizing a renewable material.

ACKNOWLEDGMENTS

This study was supported by a National Research Foundation of Korea (NRF) grant funded by the Korean government (MSIT) (NRF-2021R1A2C4001777 and NRF-2022M3H4A1A04098822). This work was also supported by the R&D Program for Forest Science Technology (FTIS2020216B10-2022-AC01), offered by the Korea Forest Service (Korea Forestry Promotion Institute). Additionally, this research was supported by the Korea Institute for Advancement of Technology (KIAT) grant funded by the Korea Government (MOTIE) (P0008458, The Competency Development Program for Industry Specialist).

REFERENCES CITED

An, L., Si, C., Bae, J. H., Jeong, H., and Kim, Y. S. (2020). "One-step silanization and amination of lignin and its adsorption of Congo red and Cu(II) ions in aqueous solution," *Int. J. Biol. Macromol.* 159, 222-230. DOI: 10.1016/j.ijbiomac.2020.05.072

Chen, W.-J., Zhao, C.-X., Li, B.-Q., Yuan, T.-Q., and Zhang, Q. (2022). "Lignin-derived materials and their applications in rechargeable batteries," *Green Chemistry* 24(2), 565-584. DOI: 10.1039/D1GC02872C

Chen, Y., Yue, M., Liu, C., Zhang, H., Yu, Y., Li, X., and Zhang, H. (2019). "Long cycle life lithium metal batteries enabled with upright lithium anode," *Advanced Functional Materials* 29(15), article 1806752. DOI: 10.1002/adfm.201806752

Das, D., Manna, S., and Puravankara, S. (2023). "Electrolytes, additives and binders for NMC cathodes in Li-ion batteries - A review," *Batteries* 9(4), article 193.

Fan, L., Shi, Z., Ren, Q., Yan, L., Zhang, F., and Fan, L. (2021). "Nitrogen-doped lignin based carbon microspheres as anode material for high performance sodium ion batteries," *Green Energy & Environ.* 6(2), 220-228. DOI: 10.1016/j.gee.2020.06.005

Heo, J. W., An, L., Chen, J., Bae, J. H., and Kim, Y. S. (2022). "Preparation of amine-functionalized lignins for the selective adsorption of methylene blue and Congo red," *Chemosphere* 295, article 133815.

Huang, F., Li, D., Wang, L., Zhang, K., Fu, L., Guo, Z., Liang, M., Wang, B., Luo, D., and Li, B. (2021). "Rational introduction of nitridizing agent to hydrothermal carbonization for enhancing CO_2 capture performance of tobacco stalk-based porous carbons," *J. Anal. Appl. Pyrol.* 157, article 105047. DOI: 10.1016/j.jaap.2021.105047

Huang, J.-Q., Zhang, Q., and Wei, F. (2015). "Multi-functional separator/interlayer system for high-stable lithium-sulfur batteries: Progress and prospects," *Energy Storage Materials* 1, 127-145. DOI: 10.1016/j.ensm.2015.09.008

Inagaki, M., Toyoda, M., Soneda, Y., and Morishita, T. (2018). "Nitrogen-doped carbon materials," *Carbon* 132, 104-140. DOI: 10.1016/j.carbon.2018.02.024

Janek, J., and Zeier, W. G. (2016). "A solid future for battery development," *Nature Energy* 1(9), article 16141. DOI: 10.1038/nenergy.2016.141

Kun, D., and Pukanszky, B. (2017). "Polymer/lignin blends: Interactions, properties, applications," *Eur. Polym. J.* 93, 618-641. DOI: 10.1016/j.eurpolymj.2017.04.035

Kwon, H. M., Kim, N. H., Hong, S. J., Sim, W. H., Lee, M., Son, S., Bae, K. Y., Kim, J. Y., Youn, D. H., Kim, Y. S., and Jeong, H. M. (2024). "Uniform Li-metal growth on renewable lignin with lithiophilic functional groups derived from wood for high-performance Li-metal batteries," *Surfaces and Interfaces* 44, article 103643.

Lazar, P., Mach, R., and Otyepka, M. (2019). "Spectroscopic fingerprints of graphitic, pyrrolic, pyridinic, and chemisorbed nitrogen in N-doped graphene," *The Journal of Physical Chemistry C* 123(16), 10695-10702. DOI: 10.1021/acs.jpcc.9b02163

Lee, H., Song, J., Kim, Y.-J., Park, J.-K., and Kim, H.-T. (2016). "Structural modulation of lithium metal-electrolyte interface with three-dimensional metallic interlayer for high-performance lithium metal batteries," *Scientific Reports* 6(1), article 30830. DOI: 10.1038/srep30830

Li, N.-W., Yin, Y.-X., Yang, C.-P., and Guo, Y.-G. (2016). "An artificial solid electrolyte interphase layer for stable lithium metal anodes," *Advanced Materials* 28(9), 1853-1858. DOI: 10.1002/adma.201504526

Li, W., Erickson, E. M., and Manthiram, A. (2020). "High-nickel layered oxide cathodes for lithium-based automotive batteries," *Nature Energy* 5(1), 26-34. DOI:

10.1038/s41560-019-0513-0

Liu, S., Wu, S., and Cheng, H. (2023). "Preparation and characterization of lignin-derived nitrogen-doped hierarchical porous carbon for excellent toluene adsorption performance," *Industrial Crops and Products* 192, article 116120. DOI: 10.1016/j.indcrop.2022.116120

Ma, S. L., Xu, B., Xu, K. W., Wu, X. L., and Chu, P. K. (2007). "Annealing behavior and hardness enhancement of amorphous SiCN thin films," *Journal of Vacuum Science & Technology A* 25(5), 1407-1410. DOI: 10.1116/1.2764080

Phothong, K., Tangsathitkulchai, C., and Lawtae, P. (2021). "The analysis of pore development and formation of surface functional groups in bamboo-based activated carbon during CO_2 activation," *Molecules* 26(18), article 5641. DOI: 10.3390/molecules26185641

Ponnusamy, V. K., Nguyen, D. D., Dharmaraja, J., Shobana, S., Banu, J. R., Saratale, R. G., Chang, S. W., and Kumar, G. (2019). "A review on lignin structure, pretreatments, fermentation reactions and biorefinery potential," *Bioresource Technol*. 271, 462-472. DOI: 10.1016/j.biortech.2018.09.070

Sani, S., Liu, X., Li, M., Stevens, L., and Sun, C. (2023). "Synthesis and characterization of three-dimensional interconnected large-pore mesoporous cellular lignin carbon materials and their potential for CO_2 capture," *Microporous and Mesoporous Materials* 347, article 112334. DOI: 10.1016/j.micromeso.2022.112334

Shi, H., Zhang, Y., Ouyang, Q., Hao, J., Huang, X., Li, J., and Chen, X. (2022). "An investigation of the structure and electrochemical performance of N-doped carbon anodes derived from poly (acrylonitrile-co-itaconic acid) /pyrolytic lignin/zinc borate," *Electrochimica Acta* 429, article 141018. DOI: 10.1016/j.electacta.2022.141018

Shokrani Havigh, R., and Mahmoudi Chenari, H. (2022). "A comprehensive study on the effect of carbonization temperature on the physical and chemical properties of carbon fibers," *Scientific Reports* 12(1), article 10704. DOI: 10.1038/s41598-022-15085-x

Sim, W. H., and Jeong, H. M. (2020). "Efficient lithium growth control from ordered nitrogen-chelated lithium-ion for high performance lithium metal batteries," *Adv. Sci. (Weinh)* 8(1), article 2002144. DOI: 10.1002/advs.202002144

Sim, W. H., and Jeong, H. M. (2021). "Lithium-metal electrodes: Efficient lithium growth control from ordered nitrogen-chelated lithium-ion for high performance lithium metal batteries." *Advanced Science* 8(1), article 2170001.

Soboleva, T., Zhao, X., Malek, K., Xie, Z., Navessin, T., and Holdcroft, S. (2010). "On the micro-, meso-, and macroporous structures of polymer electrolyte membrane fuel cell catalyst layers," *ACS Appl Mater Interfaces* 2(2), 375-384. DOI: 10.1021/am900600y

Togasaki, N., Momma, T., and Osaka, T. (2014). "Enhancement effect of trace H_2O on the charge–discharge cycling performance of a Li metal anode," *Journal of Power Sources* 261, 23-27. DOI: 10.1016/j.jpowsour.2014.03.040

Tung, S.-O., Ho, S., Yang, M., Zhang, R., and Kotov, N. A. (2015). "A dendrite-suppressing composite ion conductor from aramid nanofibres," *Nature Communications* 6(1), article 6152. DOI: 10.1038/ncomms7152

Wang, H., Pu, Y., Ragauskas, A., and Yang, B. (2019). "From lignin to valuable products-strategies, challenges, and prospects," *Bioresource Technol*. 271, 449-461. DOI: 10.1016/j.biortech.2018.09.072

Wang, J., Fan, D., Zhang, L., Yang, D., Qiu, X., and Lin, X. (2023). "Lignin-derived hierarchical porous carbon with high surface area and interconnected pores for efficient antibiotics adsorption," *Chemical Engineering Journal* 454, article 139789. DOI: 10.1016/j.cej.2022.139789

Wei, Q., Tong, X., Zhang, G., Qiao, J., Gong, Q., and Sun, S. (2015). "Nitrogen-doped carbon nanotube and graphene materials for oxygen reduction reactions," *Catalysts* 5(3), 1574-1602. DOI: 10.3390/catal5031574

Won, J. H., Sim, W. H., Kim, D., and Jeong, H. M. (2023). "Densely packed Li-metal growth on anodeless electrodes by Li(+) -flux control in space-confined narrow gap of stratified carbon pack for high-performance Li-metal batteries," *Adv. Sci. (Weinh)* 10(3), article e2205328.

Wu, J., Pan, Z., Zhang, Y., Wang, B., and Peng, H. (2018). "The recent progress of nitrogen-doped carbon nanomaterials for electrochemical batteries," *Journal of Materials Chemistry A* 6(27), 12932-12944. DOI: 10.1039/C8TA03968B

Xu, S., Chen, K.-H., Dasgupta, N. P., Siegel, J. B., and Stefanopoulou, A. G. (2019). "Evolution of dead lithium growth in lithium metal batteries: Experimentally validated model of the apparent capacity loss," *Journal of The Electrochemical Society* 166(14), A3456-A3463. DOI: 10.1149/2.0991914jes

Xu, W., Wang, J., Ding, F., Chen, X., Nasybulin, E., Zhang, Y., and Zhang, J.-G. (2014). "Lithium metal anodes for rechargeable batteries," *Energy & Environmental Science* 7(2), 513-537. DOI: 10.1039/C3EE40795K

Yan, B., Zheng, J., Feng, L., Zhang, Q., Zhang, C., Ding, Y., Han, J., Jiang, S., and He, S. (2023). "Pore engineering: Structure-capacitance correlations for biomass-derived porous carbon materials," *Materials & Design* 229, article 111904. DOI: 10.1016/j.matdes.2023.111904

Yan, Z. (2023). "Symmetric cells as an analytical tool for battery research: Assembly, operation, and data analysis strategies," *Journal of The Electrochemical Society* 170(2). DOI: 10.1149/1945-7111/acaf42

Yang, C., Fu, K., Zhang, Y., Hitz, E., and Hu, L. (2017). "Protected lithium-metal anodes in batteries: From liquid to solid," *Advanced Materials* 29(36), article 1701169.

Yu, J., Dang, Y., Bai, M., Peng, J., Zheng, D., Zhao, J., Li, L., and Fang, Z. (2019). "Graphene-modified 3D copper foam current collector for dendrite-free lithium deposition," *Frontiers in Chemistry* 7. DOI: 10.3389/fchem.2019.00748

Yue, X.-Y., Wang, W.-W., Wang, Q.-C., Meng, J.-K., Zhang, Z.-Q., Wu, X.-J., Yang, X.-Q., and Zhou, Y.-N. (2018). "CoO nanofiber decorated nickel foams as lithium dendrite suppressing host skeletons for high energy lithium metal batteries," *Energy Storage Materials* 14, 335-344. DOI: 10.1016/j.ensm.2018.05.017

Zhang, W., Qiu, X., Wang, C., Zhong, L., Fu, F., Zhu, J., Zhang, Z., Qin, Y., Yang, D., and Xu, C. C. (2022). "Lignin derived carbon materials: Current status and future trends," *Carbon Research* 1(1), article 14. DOI: 10.1007/s44246-022-00009-1

Zheng, G., Lee, S. W., Liang, Z., Lee, H.-W., Yan, K., Yao, H., Wang, H., Li, W., Chu, S., and Cui, Y. (2014). "Interconnected hollow carbon nanospheres for stable lithium metal anodes," *Nature Nanotechnology* 9(8), 618-623. DOI: 10.1038/nnano.2014.152

Zheng, L., Wang, X., Wang, H., Zhao, X., Kong, F., and Liu, Y. (2022). "Novel nitrogen-doped porous carbon with high surface areas prepared from industrial alkali lignin for supercapacitors," *ChemElectroChem* 9(24), article e202200869. DOI: 10.1002/celc.202200869

Zou, G., Zhang, D., Dong, C., Li, H., Xiong, K., Fei, L., and Qian, Y. (2006). "Carbon nanofibers: Synthesis, characterization, and electrochemical properties," *Carbon* 44(5), 828-832. DOI: 10.1016/j.carbon.2005.10.035

Article submitted: October 27, 2023; Peer review completed: November 30, 2023; Revised version received and accepted: December 5, 2023; Published: December 15, 2023.
DOI: 10.15376/biores.19.1.1010-1029

APPENDIX
Supplementary

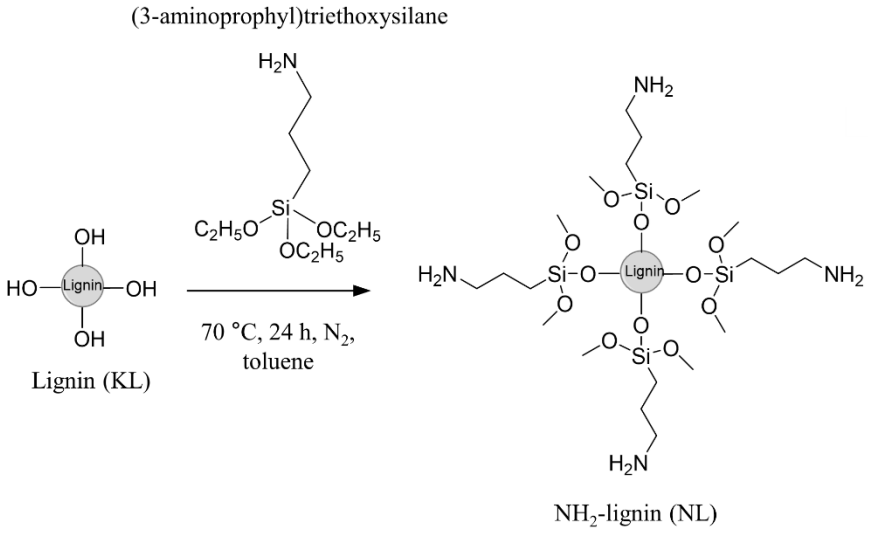

Fig. S1. Synthesis process of NH_2-lignin (NL) from a kraft lignin (KL)

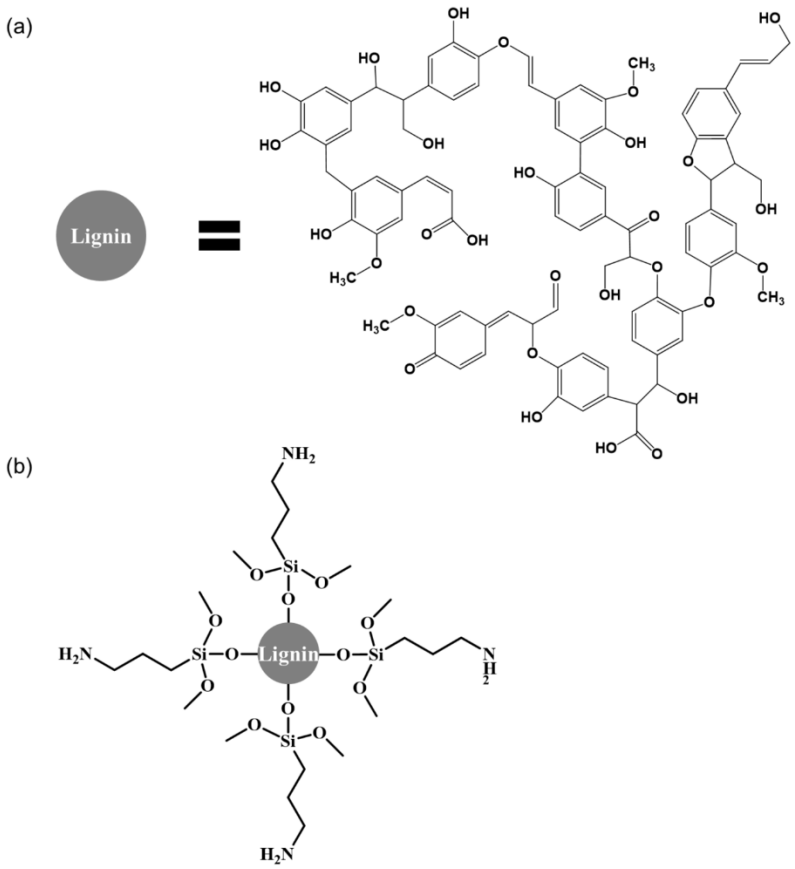

Fig. S2. (a) Molecular structure of a kraft lignin (KL) (Kun and Pukanszky 2017), and (b) NH_2-lignin (NL) used in this paper

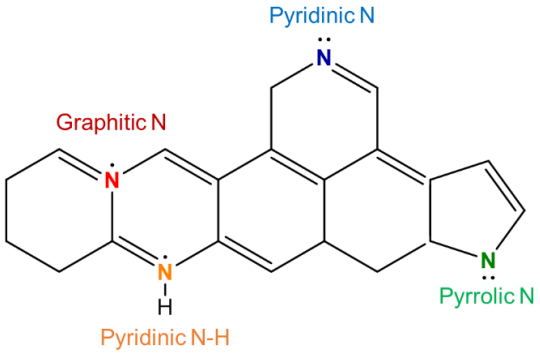

Fig. S3. Examples of lithiophilic N atoms within carbonaceous materials

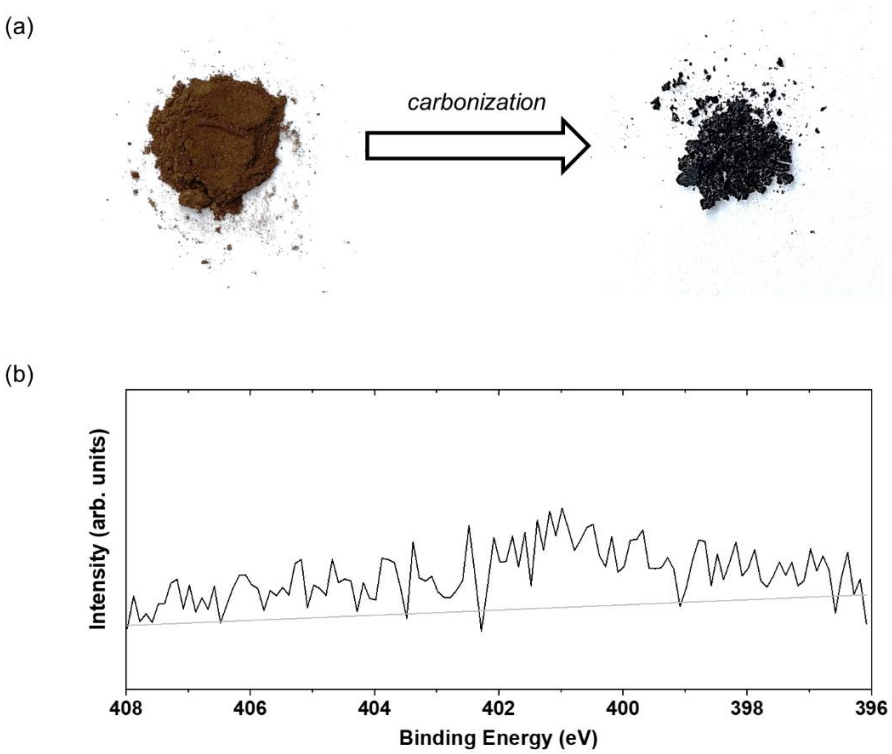

Fig. S4. (a) Images of kraft lignin (KL) and carbonized kraft lignin (KLC);
(b) Investigation of XPS for the N element of kraft lignin carbon (KLC)

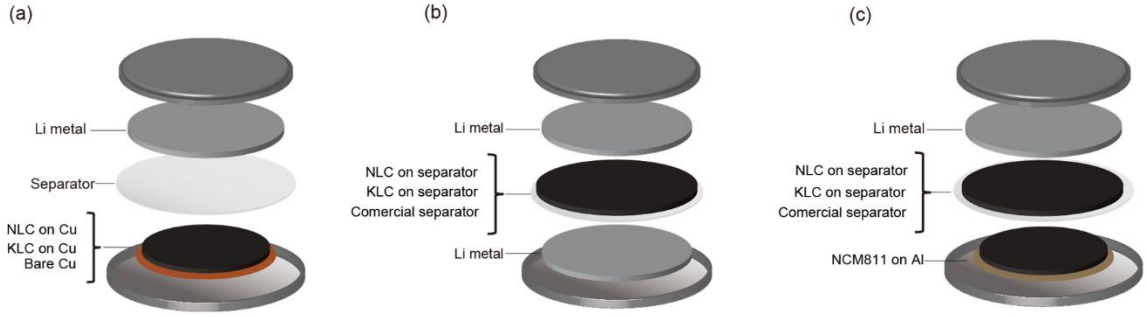

Fig. S5. Schematic illustrations of a battery configuration for the electrochemical tests: (a) half-cell; (b) symmetric cell, and (c) full cell

Table S1. Element Contents and Molecular Weight of Kraft Lignin (KL) and NH_2-lignin Used in this Paper

	C (%)	H (%)	N (%)	O (%)	S (%)	Average molecular weight		
						M_n (g/mol)	M_w (g/mol)	M_w/ M_n
Kraft lignin	66.2	6.37	0.02	27.37	0.04	4000	6400	1.60
NH_2-lignin	45.67	6.13	2.53	45.66	0.00	4700	8300	1.77